Macromolecular Materials and Engineering
www.mme-journal.de

Co-Culture of Keratinocyte-*Staphylococcus aureus* on Cu-Ag-Zn/CuO and Cu-Ag-W Nanoparticle Loaded Bacterial Cellulose:PMMA Bandages

*Esra Altun, Mehmet Onur Aydogdu, Maryam Crabbe-Mann, Jubair Ahmed, Francis Brako, Betul Karademir, Burak Aksu, Muge Sennaroglu, Mehmet S. Eroglu, Guogang Ren, Oguzhan Gunduz, and Mohan Edirisinghe**

Pressurized gyration and its sister processes are novel methods to produce polymeric fibers. Potential applications for such fibers include wound dressings, tissue engineering scaffolds, and filters. This study reports on a pressurized gyration technique that employs pressured N_2 gas to prepare biocompatible wound dressing bandages from bacterial cellulose and poly (methylmethacrylate) polymer blended with alloyed antimicrobial nanoparticles. Resulting bandages are manufactured with high product yield and characterized for their chemical, physical, and mechanical properties. Increased density in solutions with additional antimicrobial nanoparticles results in increased fiber diameters. Also, addition of antimicrobial nanoparticles enhances ultimate tensile strength and Young's modulus of the bandages. Typical molecular bonding in the bandages is confirmed by Fourier-transform infrared spectroscopy, with peaks that have higher intensity and narrowing points being caused by additional antimicrobial nanoparticles. More so, the cellular response to the bandages and the accompanying antimicrobial activity are studied in detail by in vitro co-culture of *Staphylococcus aureus* and keratinocytes. Antimicrobial nanoparticle-loaded bandage samples show increased cell viability and bacteria inhibition during co-culture and are found to have a promising future as epidermal wound dressing materials.

1. Introduction

Wound dressings are continuously evolving since ancient times, from using natural materials, such as honey pastes, plant fibers, and animal fats to more sophisticated wound dressings at present.[1] More recently wound dressings have developed into more complex forms in terms of materials and methods used, where a combination of physical and biochemical features of natural and synthetic polymers have resulted in the concept of contemporary wound dressings.[2] Each method relies on creating the most beneficial material combination to be used as a wound dressing with the purpose of creating an optimal environment for re-establishing each layer of the skin. Therefore, a proper wound dressing needs to work according to the fundamental functions of the native human skin by preventing infection and dehydration, and simultaneously supporting the self-regeneration abilities of

E. Altun, M. O. Aydogdu
Advanced Nanomaterials Research Laboratory
Department of Metallurgical and Materials Engineering
Institute of Pure and Applied Sciences
Marmara University
Goztepe Campus, 34722 Istanbul, Turkey
M. Crabbe-Mann, J. Ahmed, Dr. F. Brako, Prof. M. Edirisinghe
Department of Mechanical Engineering
University College London
Torrington Place, WC1E 7JE London, UK
E-mail: m.edirisinghe@ucl.ac.uk
The ORCID identification number(s) for the author(s) of this article can be found under https://doi.org/10.1002/mame.201800537.

DOI: 10.1002/mame.201800537

Dr. B. Karademir
Department of Medical Biochemistry
School of Medicine, Marmara University
Basibuyuk Campus, 34854 Istanbul, Turkey
Dr. B. Aksu
Department of Medical Microbiology
School of Medicine, Marmara University
Basibuyuk Campus, 34854 Istanbul, Turkey
Dr. M. Sennaroglu, Prof. M. S. Eroglu
Department of Chemical Engineering
Faculty of Engineering, Marmara University
Goztepe Campus, 34722 Istanbul, Turkey
Dr. G. Ren
Science and Technology Research Institute
University of Hertfordshire
Hatfield, AL10 9AB Hertfordshire, UK
Dr. O. Gunduz
Advanced Nanomaterials Research Laboratory
Department of Metallurgical and Materials Engineering
Faculty of Technology, Marmara University
Goztepe Campus, 34722 Istanbul, Turkey

the skin such as cell proliferation, migration, and epithelization, which are being observed as physiological phenomenon to compensate with compromised integrity of the skin.[3,4] Not only limited within these aspects, active compounds can also increase the efficiency of wound dressings. As an example, introduction of antimicrobial nanoparticles such as silver or copper to the wound dressing resulted in enhancing the antimicrobial capabilities which is crucial in protecting a wound area from pathological invaders, a condition that can dramatically impede the regeneration process.[5–7] Therefore, as attempted in the present work, considering the foregoing, incorporation of a natural polymer with a synthetic polymer and enhancing them with antimicrobial nanoparticles can be a very promising combination for epidermal wound dressing studies.

Bacterial cellulose (BC) is a natural polymer with good mechanical properties and water absorption ability,[8] and is considered to be a promising wound healing material.[9,10] Nevertheless, manufacturing scaffold-like bandages from BC alone is very difficult and yield can be insufficient.[11] BC is a pellicle-formed polymer and it can only be used after physical fragmentation which is helped by the gyration method[12] without any chemical process to protect its own polymeric feature. Fragmented BC particles are not able to reunite and should be immersed in a polymer solution. By doing that multiple layers of water surrounding polyglucosan chains of BC would be displaced, inducing the formation of bonds between BC and polymer, with consequent marked structural modification. Poly (methylmethacrylate) (PMMA) is an easily processable synthetic polymer with low toxicity.[12] PMMA is also reported for its synergy with the surrounding environment features, by providing a strong physical structure to fill in gaps and hydrophobicity,[13] but it is quite brittle.[14] Therefore, blending PMMA with BC can overcome the individual weaknesses of BC and PMMA to create a valuable material combination, which meets the requirements of the wound dressing concept.

Ag and Cu nanoparticles (NPs) exhibit a multilevel antibacterial effect on cells. These make them both effective, individually or as combined mixtures, particularly as new antimicrobials. Many studies on Ag NPs and Cu NPs have addressed the treatment of multidrug-resistant species by using Ag NPs, where last resort antibiotics have failed to contain the infection. Some pioneering work by Ren and co-workers.,[15–17] on Ag, Cu, and other metal nanocomposites against methicillin-resistant *Staphylococcus aureus* (MRSA) demonstrated significant minimum inhibitory concentration (MIC) reduction and killing rate (99.999%). At the same time, the Ag-Cu NP combinations are able to kill a wider spectrum of bacteria and are expected to reduce inflammation as well as allow for better wound healing with minimal tissue scarring.[18–20] Due to the above-mentioned reasons, antimicrobial nanoparticles including Ag-Cu NPs namely, UHNP-1 and AVNP-2 were added to wound dressing bandages and bacteria inhibition is examined along with keratinocyte viability and proliferation using co-culture. UHNP-1 is a combination of Ag NPs (20–50 nm) and Cu NPs (10–30 nm) and used for enhanced antimicrobial properties, whereas AVNP-2 (20–70 nm) was a combination of Ag NPs, Cu NPs, WC NPs, and carbon NPs. The majority of the constituents in AVNP-2 were intended to increase the synergistic effect between Ag-Cu and carbon NPs. A high-level content of sp^2 C—C powder in AVNP-2 was used for achieving a significant reduction in cell toxicity.[15–17,21,22]

Wound dressing manufacture requires the generation of fiber mat bandages with high yield. A novel method of production, pressurized gyration, which is based on production of polymeric fibers using the application of centrifugal force and dynamic fluid flow under pressure has resulted in significant results compared to other methods (e.g., electrospinning). The method is electro- and/or magnetic-field-free and a nozzle-free technique in forming a web of polymeric fibers in large scale.[23–25] Furthermore, our previous work has reported successful results (nanometer scaled fibers, high product yield in one step, remarkable biocompatibility and cell proliferation on scaffolds, better tensile strain than electrospun BC:PMMA scaffolds and increased water absorption capacity) with respect to BC:PMMA wound dressing bandage fabrication.[12] The present work capitalizes on these findings[12] and describes an in-depth investigation on BC:PMMA bandage like scaffolds, as well as widening the concept by adding antimicrobial nanoparticles into the composite structure. Bandages were tested for chemical, morphological, and mechanical properties. Most importantly, gyrospun BC bandages were tested by in vitro co-culture of *S. aureus* and keratinocytes to evaluate the antimicrobial and cytotoxicity performance of the bandages.

2. Experimental Section

2.1. Materials

BC was provided by the Department of the Medical Microbiology, Medipol University (Istanbul, Turkey). PMMA (MW = 12×104 g mol^{-1}), dimethylformamide (DMF), and tetrahydrofuran (THF) were obtained from Sigma-Aldrich (Gillingham, UK). Antimicrobial nanoparticles (two different types: UHNP-1 and AVNP-2) 1 wt/vol% in chloroform were provided by the University of Hertfordshire, UK. The contents were Cu-Ag-Zn/CuO in the case of UHNP-1 and Cu-Ag-WC in AVNP-2. More details are given elsewhere.[22,26]

2.2. Preparation of Blend Solutions

5 wt% BC was sonicated in DMF:THF (50:50 wt ratio) using a sonifier (Branson Sonifier 250, BRANSON Ultrasonics Corporation, USA) at a power output of 100% for 1 h. To prepare PMMA solution, 50 wt% PMMA polymer was dissolved in DMF:THF solution (50:50 wt ratio) in airtight vial using a magnetic stirrer for 3 h at 50 °C. Prepared BC and PMMA solutions were blended in 2:5 wt ratio and magnetically stirred for 1 h at the ambient temperature (23 °C). UHNP-1 and AVNP-2 were added to the obtained BC:PMMA polymer solution at various concentrations (0.05, 0.1, 0.5, and 1 wt%). Finally, UHNP-1 and AVNP-2 containing solutions were magnetically stirred for 1 h at the ambient temperature

and immediately used in experiments. The BC:PMMA ratio and procedure were selected as a result of the outcomes in preliminary investigations.[12]

2.3. Pressurized Gyration

Schematic representation of the gyration apparatus is shown in **Figure 1**A. The system consists of a rotary aluminum cylindrical vessel approximately 60 mm in diameter and 35 mm in height. It also has 20 small round orifices of 0.5 mm diameter in size, which are distributed evenly in a line on its surface. A rotary joint was attached to the lid at top of the vessel to establish connection to the pressurized gas. Regulator was also used to control the flow rate of N_2 gas pressure, which can be varied up to 3×10^5 Pa. High speed DC rotary motor attached to the bottom end of the cylindrical vessel was connected to the circuit board, which enables the control over apparent rotation speed up to 36 000 rpm. The lid was tightly screwed to the vessel in order to prevent any possible leak between the lid and the vessel since all polymer solution needs to be transferred via orifices in order to keep the uniform structure of the fibers. The apparatus was placed in a protective cabinet and supported with a stainless steel collection plate positioned 50 mm away from the orifices.

Polymer solution comes out from the cylindrical vessel because of the centrifugal force which is created by the high speed of the rotation movement and then transformed into a jet. While forming the polymer jet, solvents were rapidly evaporated and fiber mesh was obtained and a photograph of the system post process is shown in Figure 1B. Bracelet like bandages made from BC:PMMA:UHNP-1 and BC:PMMA:AVNP-2 blend solutions were collected in 15 s and used in characterization tests. All experiments were conducted accordingly to the preliminary work of this study,[12] using a fixed rotation speed of 36 000 rpm at a working pressure of 3×10^5 Pa at ambient temperature (23 °C) and 51–58% relative humidity. After gyration, a vacuum oven was used to evaporate residual solvents that may have remained in the bandages.

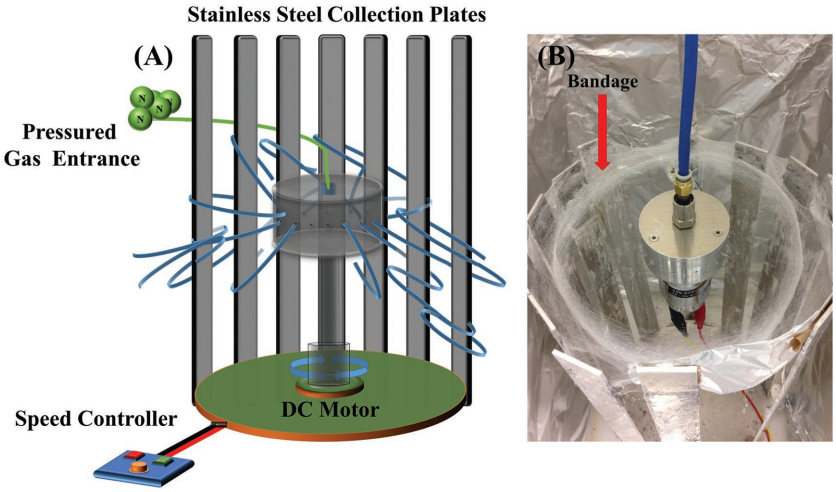

Figure 1. Pressurized gyration apparatus: A) schematic representation of the pressurized gyration process and B) image of the system after pressurized gyration process.

2.4. Characterization

2.4.1. Calculations of Density and Yield

Density of the solutions were measured using a standard 5 mL density bottle and all measurements were repeated five times. Yield of the pressurized gyration processes were determined with following equation and all evaluations were repeated five times:

$$\%\text{Yield} = 100\ (\text{Obtained solid product weight (g)}/\text{Loaded solutions weight (g)}) \quad (1)$$

2.4.2. Scanning Electron Microscopy

The surface morphologies of the bandages were studied using a scanning electron microscope (SEM, MA EVO 10, ZEISS, US) using an accelerating voltage of 10 kV. Samples were sputter coated with gold for 60 s using a Quorum SC7620 Mini Sputter Coater before imaging. Additionally, the SEM instrument was equipped with energy dispersive X-ray (EDX) for performing compositional analysis. Structural features of bandages were studied using a JASCO FT/IR-4000 spectrometer (JASCO, Japan) in transmittance mode. Fourier-transform infrared spectroscopy (FTIR) spectra of the bandages were taken at 4 cm^{-1} resolution over the range 4000–400 cm^{-1}.

2.4.3. Determination of Mechanical Properties

Thickness of each bandage sample was measured five times at different points using a high-accuracy digital micrometer

Table 1. Density of the solutions prepared, relative humidity values used in gyration experiments and percentage yields with standard deviations obtained. All data represents mean ± SD. (Sample quantity used = 5, Pressure used = 3×10^5 Pa, Rotation speed = 36 000 rpm and Temperature = 23 °C).

Sample name	Density [kg m^{-3}]	Relative humidity [%]	Yield [%]
BC:PMMA	1050 ± 0.5	53.8 ± 0.3	50 ± 0.5
0.05 UHNP-1	1040 ± 0.1	54.8 ± 0.1	56 ± 2
0.1 UHNP-1	1050 ± 0.1	56.5 ± 0.2	25 ± 1
0.5 UHNP-1	1080 ± 0.3	54.6 ± 0.4	46 ± 0.3
1 UHNP-1	1140 ± 0.7	54.1 ± 0.1	61 ± 0.7
0.05 AVNP-2	1040 ± 0.1	54.1 ± 0.3	49 ± 1
0.1 AVNP-2	1050 ± 0.2	55.8 ± 0.2	27 ± 1.5
0.5 AVNP-2	1080 ± 0.5	52.7 ± 0.5	67 ± 0.5
1 AVNP-2	1150 ± 0.6	53.9 ± 0.3	46 ± 0.8

(Mitutoyo, High-Accuracy Digimatic Micrometer, USA). Average thickness value of each sample was used for tensile strength determinations. Uniaxial tensile testing was performed using a tensile strength measurement device (INSTRON 4411, Mass., USA). All tests were conducted at the ambient temperature (23 °C) at a crosshead speed of 5 mm min^{-1} and 30 mm gauge length and repeated five times. Furthermore, Young's modulus, which is an important parameter for evaluating the flexibility of the bandage scaffolds and elongation at break were calculated from the stress–strain graphic generated.

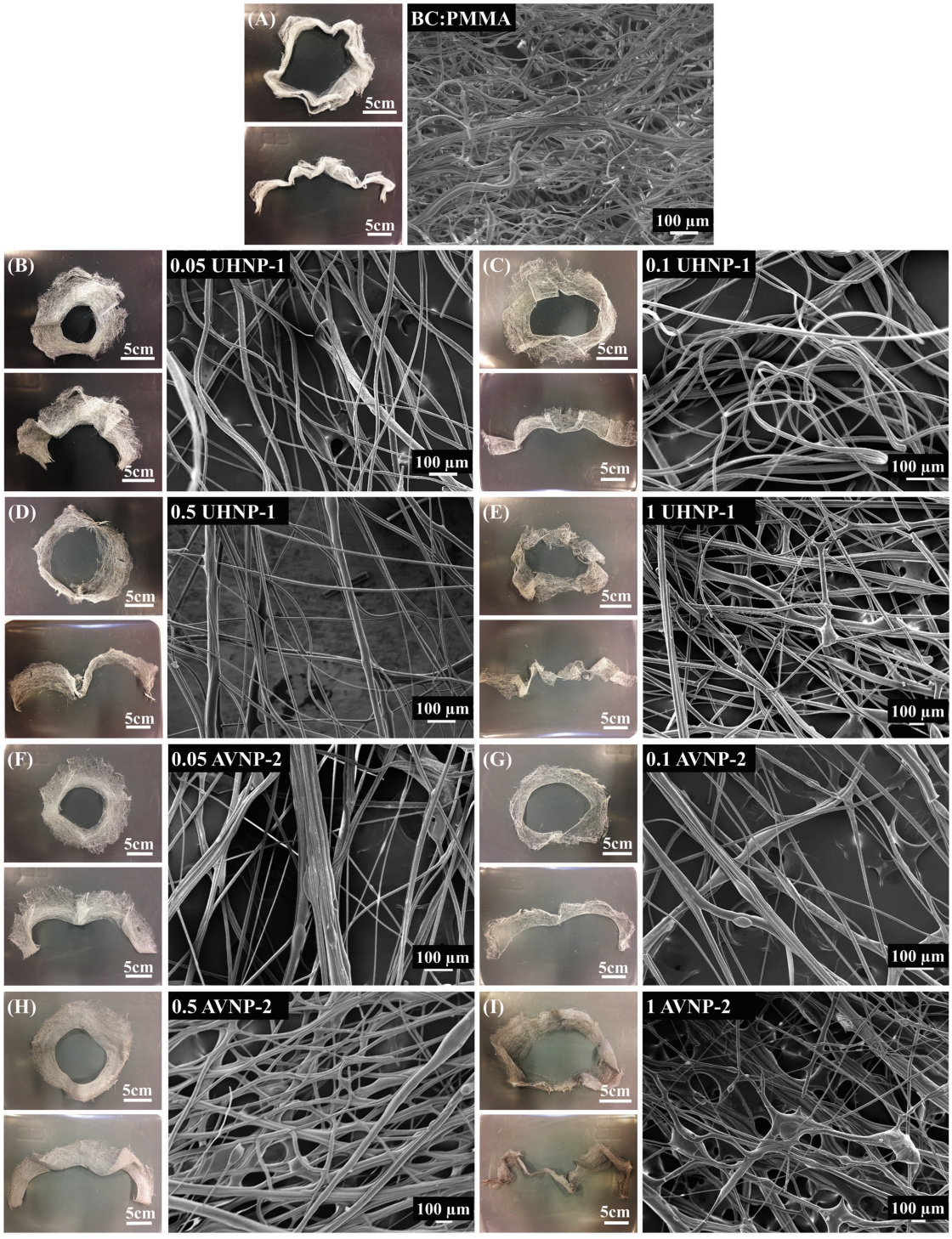

Figure 2. Macro photo and SEM images of bandage samples corresponding to Table 1: A) BC:PMMA, B) 0.05 UHNP-1, C) 0.1 UHNP-1, D) 0.5 UHNP-1, E) 1 UHNP-1, F) 0.05 AVNP-2, G) 0.1 AVNP-2, H) 0.5 AVNP-2, and I) 1 AVNP-2.

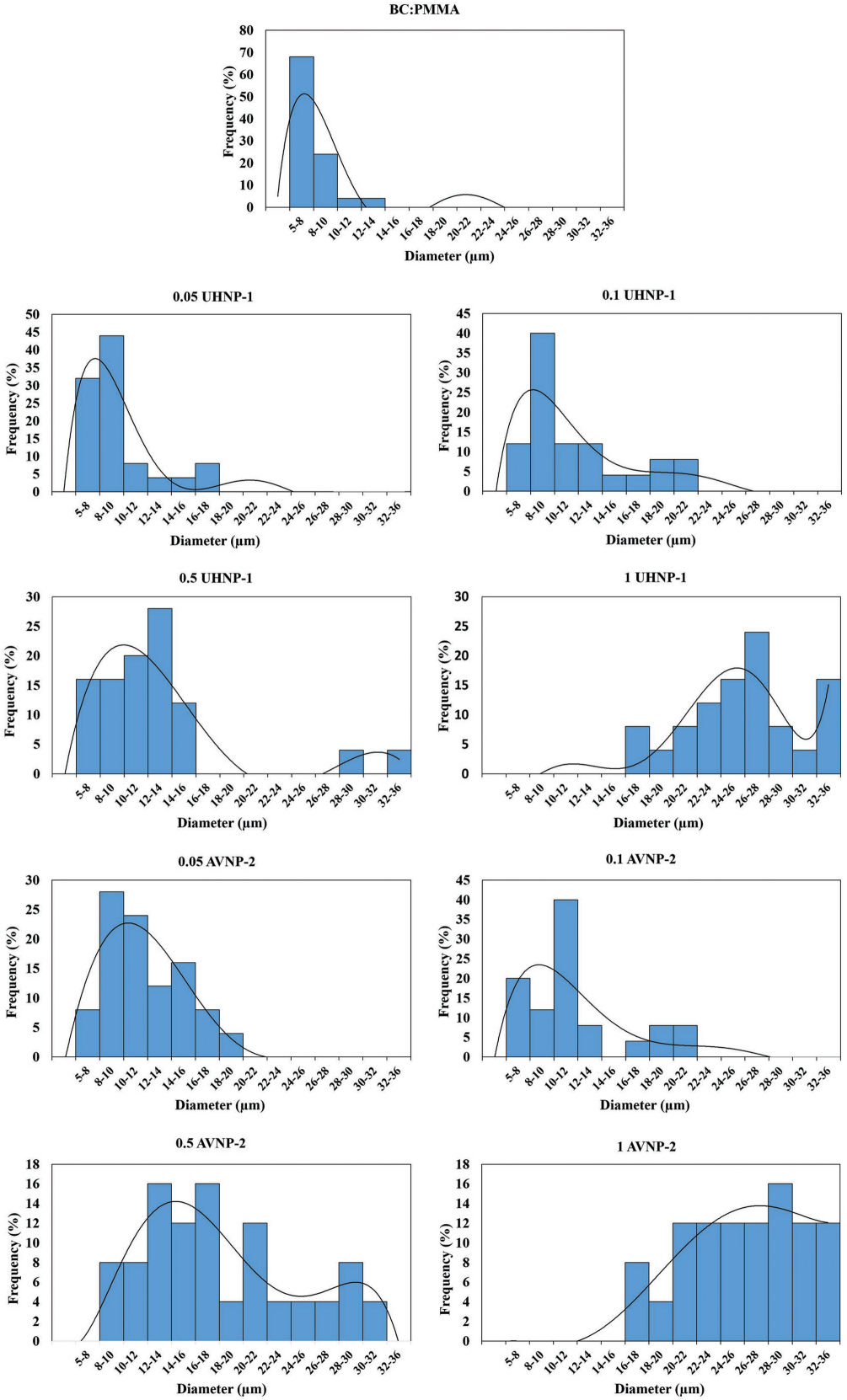

Figure 3. Fiber size distribution graphs of produced bandages

2.4.4. Determination of Water Uptake and Weight Loss Capabilities

The water uptake UHNP-1 and AVNP-2 loaded BC:PMMA bandage samples of 20 mg (W_d) was determined by immersing the bandages in phosphate buffer saline (PBS), (pH 7.4 and 4) at 37 °C. At predetermined time intervals (1, 3, 5, 7, 9, 12, and 15 days), the bandage samples were taken out from the medium and excess fluid remaining on the surface was gently removed by filter paper. Subsequently, the wet weight of the sample (W_s) was measured. Tests were repeated five times. The water uptake ability of the bandages was calculated as follows:

$$\%\text{Water uptake} = 100(W_s - W_d)/W_d \quad (2)$$

To examine the biodegradation, all bandage samples with known weight (W_0, 20 mg) were placed in a test tube containing 4 mL PBS (pH 7.4 and pH 4), followed by incubation for 15 days at 37 °C. After each predetermined time point (1, 3, 5, 7, 9, 12, and 15 days), the bandage samples were removed from the PBS medium, washed with distilled water, kept at vacuum oven for 24 h and then weighted (W_f) to calculate their weight loss. Tests were repeated five times. The weight loss of the bandage samples was calculated as

$$\%\text{Weight Loss} = 100(W_f - W_0)/W_0 \quad (3)$$

2.4.5. Differential Scanning Calorimetry

Differential scanning calorimetry (DSC) was used to determine the glass transition temperature (T_g) of the bandage samples. Perkin–Elmer Thermal Analyzer System (PerkinElmer Inc., Mass., USA) equipped with Jude DSC system was used. Prior to the analyses, samples were kept in a vacuum oven at 50 °C for 48 hours to evaporate residual solution in the bandage samples. Measurements were performed at 10 °C min^{-1} under a dynamic argon atmosphere (200 mL min^{-1}). The temperature and enthalpy calibrations of the instrument were performed according to the indium and zinc melting points and melting enthalpies. About 7 mg of sample was used in each measurement. The obtained data was analyzed using associated computer software (Pyris, PerkinElmer Inc., Mass., USA).

2.4.6. Co-Culture Testing

Before the co-culture tests the bandage samples were exposed to UV radiation for 2 h in a 6-well plate, washed three times with PBS (pH 7.4) for 20 min each and incubated with Dulbecco's modified Eagle's medium (DMEM) for 24 h before cell seeding. Keratinocytes were cultured in DMEM supplemented with penicillin (100 units per mL), streptomycin (100 µg mL^{-1}), and 10% fetal calf serum in a humidified atmosphere of 5% CO_2 and 95% air at 37 °C. After reaching 70% confluence, the cells were detached by trypsin–EDTA and viable cells were counted by trypan blue assay. Cells were further seeded onto the products at a density of 40 × 104 cells per well and cultured in the medium together with the scaffolds for 16 h to allow the attachment of the cells onto the materials. *S. aureus* ATCC29213 was grown on blood agar plates at 37 °C overnight. Bacteria was subcultured into tryptic soy broth (TSB, BD-Difco, Sparks, MD, USA) and grown for an additional 18 h at 37 °C. Cells were washed with sterile PBS (pH 7.4) twice and resuspended in PBS at 0.5 McFarland turbidity standard (approximately 10^8 CFU mL^{-1}) by using spectrophotometry at 600 nm. Following the cell attachment, bacteria were seeded onto the test samples with a multiplicity of infection (MOI), a ratio of bacteria to keratinocytes of 0.04 and incubated for 24 h, 48 h, and 72 h at 37 °C and 5% CO_2 in DMEM without antibiotics. Cell culture supernatant samples were taken after 24 h, 48 h, and 72 h incubation. Samples were serial 10-fold diluted with sterile PBS (1:100, 1:1000, and 1:10 000 dilutions). Fifty µL from each dilution was plated on tryptic soy agar (TSA, BD-Difco, Sparks, MD, USA) and incubated overnight at 37 °C. Resulting colonies were counted and the number of CFU was calculated by averaging each dilution.

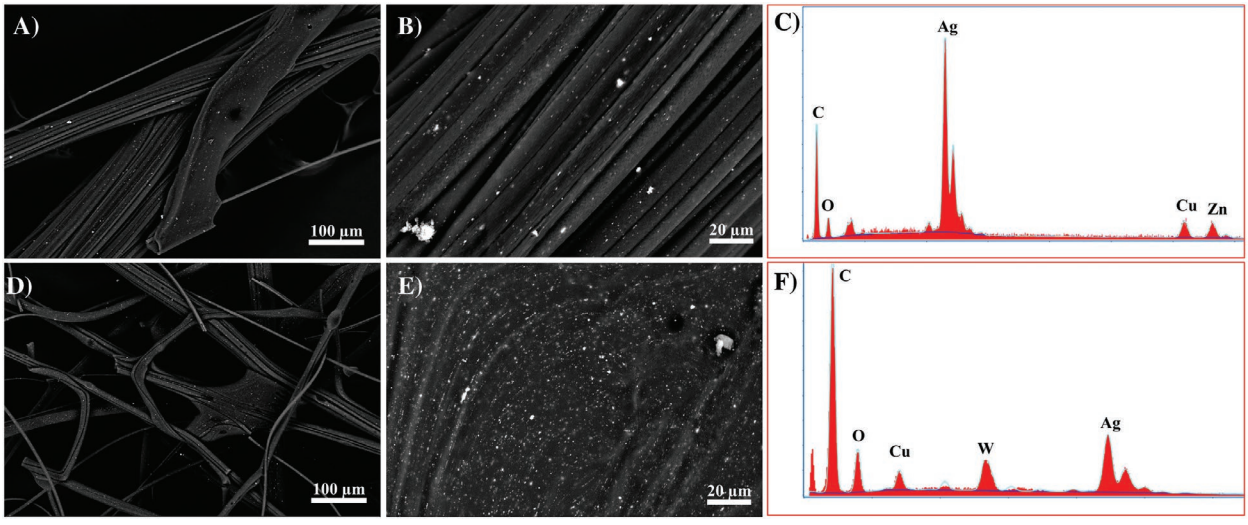

Figure 4. SEM and corresponding EDX analysis of bandage samples loaded with UHNP-1 and AVNP-2 at concentrations of 1 wt%. A–C) UHNP-1 and D–F) AVNP-2.

Cell viability was determined using MTT (3-(4,5-dimethylthiazol-2-yl)-2,5-diphenyl-2H-tetrazolium bromide) reduction by viable cells. Cells were imaged by fluorescence microscopy (DMi8, Leica, Germany) following DAPI staining of the nucleus. Materials were transferred into a new 6-well plate to eliminate any contamination.

After the co-culture test cells and bacteria were first washed with PBS and fixed with 2.5% gluteraldehyde. After that, they were washed with distilled water for 3 × 5 min, subsequently they were dehydrated through 30%, 50%, 70%, 80%, 90%, 96%, and 100% alcohol series, each lasting 5 min. Then, they were passed through 30% and 50% acetone in series for 5 min and taken to 100% acetone. Finally, samples were sputter coated with gold using a Quorum SC7620 Mini Sputter Coater for 60 s before imaging.

3. Results and Discussion

In the pressurized gyration method, fiber and bandage shape formations are reliant on the solution properties and environmental conditions along with the processing parameters.[27] **Table 1** shows how bandages produced with different increments of UHNP-1 and AVNP-2 concentrations are related to the average solution density. According to this table, increased density in solutions resulted in increased fiber diameters (**Figure 2**). On the other hand, relative humidity of the working environment was not much different for all samples. However, as Illangakoon et al.[26] explained, relative humidity is the one of the key factors controlling pressurized gyration output and at lower humidity, rate of solvent evaporation and fiber formation will be much more compared to higher humidity conditions. Lower humidity could result in the solvent drying completely and increasing the rate of solvent evaporation which may have influenced the uniformity of fibers. On the other hand, high humidity causes thicker fiber diameters to be formed.[28] In terms of obtaining overall high yield, the experimental system depends on all solution processing and ambient parameters, individually. However, the solvent will also govern the chain entanglement and it directly will affect the percentage yield of bandages.[29] Accordingly, chloroform solvents in UHNP-1 and AVNP-2 may have decreased the percentage yield of bandages.

Typical products are illustrated in **Figures 2** and **3**. Figure 2A indicates that the BC:PMMA control sample exhibits smooth and cotton-like surface texture whilst the surface texture of UHNP-1 and AVNP-2 loaded bandage samples are rougher and the surface roughness increases by increasing the amount of UHNP-1 and AVNP-2 (Figure 2B–I). Bandage samples prepared with a high antimicrobial nanoparticle loading were darker in color. Also, the fiber diameter distribution profile (Figure 3) showed a steady increase as antimicrobial nanoparticle concentration increased in the samples which is directly connected to the increased density in the bandage samples (Table 1).

The presence of the silver (Ag), copper (Cu), zinc (Zn), and tungsten (W) peaks are also confirmed by EDX spectroscopy of the relevant bandage samples. **Figure 4** shows the EDX results (shown along with SEM image) of bandage samples loaded with UHNP-1 (Figure 4A–C) and AVNP-2 (Figure 4D–F) at concentrations of 1 wt%. Using a high magnification and increased accelerating voltage in the SEM investigation, it has been revealed that the antimicrobial nanoparticles were not only embedded on the surface of the UHNP-1 and AVNP-2 samples, but that they were also located inside the fibers as a result of

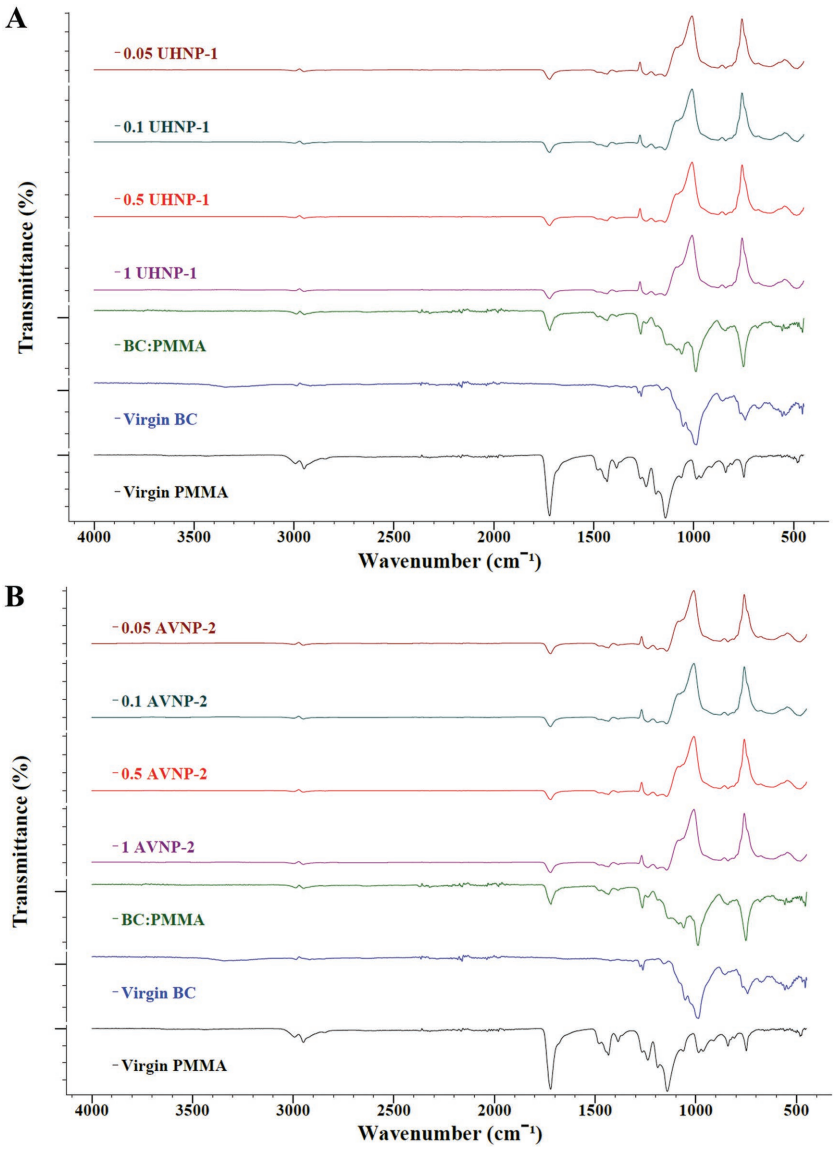

Figure 5. FTIR spectra of virgin PMMA, virgin BC, BC:PMMA, A) UHNP-1 and B) AVNP-2 bandage samples.

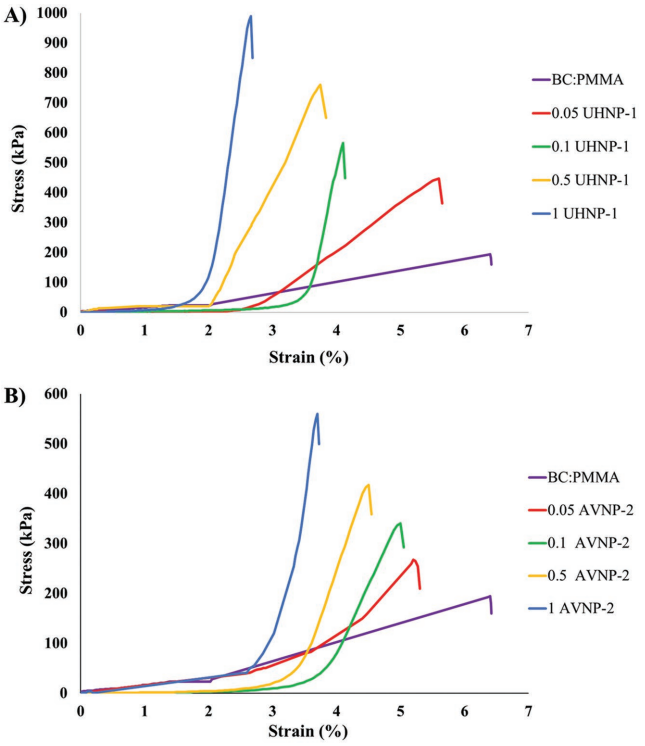

Figure 6. Stress-strain curves for gyrospun BC:PMMA bandage samples with different weight ratios of A) UHNP-1 and B) AVNP-2.

proper blending in the solution preparing phase. Elemental analysis confirmed that the UHNP-1 consists of Ag, Cu, and Zn (Figure 4C) elements while the AVNP-2 contains Cu, Ag, and W (Figure 4F).

Figure 5 shows the FTIR spectra of virgin PMMA, virgin BC, BC:PMMA, and UHNP-1 (Figure 5A) and AVNP-2 (Figure 5B) loaded bandage samples. PMMA is characterized by a broad band at 1721 cm^{-1} for stretching vibration of C=O, and the band around at 2900 cm^{-1} corresponds to the methylene C−H stretching of both BC and PMMA materials.[30,31] The bands at 1350 and 1450 cm^{-1} are associated with C-H symmetric and asymmetric stretching modes, respectively. The 1240 cm^{-1} band is assigned to antisymmetric C−C−O stretch and it seems slightly deeper in UHNP-1 and AVNP-2 bandage samples than the BC:PMMA control bandage sample, this can be caused the interaction of UHNP-1 and AVNP-2 with BC:PMMA in the bandage samples. The band at 1060 cm^{-1} is caused by the C−O−C pyranose ring skeletal vibration of BC.[32] Also, two high intensity of peaks around 1020 and 750 cm^{-1} are observed in both UHNP-1 and AVNP-2 spectra. Higher intensities can represent more absorption of light in IR region due to added antimicrobial nanoparticles. Additionally, narrowing of aforementioned peaks shows immobility of atoms in molecules due to bonding of antimicrobial nanoparticles.

The effects of the different ratios of UHNP-1 and AVNP-2 on the mechanical properties were also evaluated. Tensile tests were performed on all bandages to determine whether the tensile strength properties were favorable for use as a wound dressing which is a significant feature of these materials to improve biomechanical defense of the wound area.[33] **Figure 6** shows the typical tensile stress–strain curves of pressurized gyrated bandage samples. The ultimate tensile strength, Young's modulus and percentage elongation at break are summarized in **Table 2**. It can be seen that the UHNP-1 (Figure 6A) loaded bandage samples showed higher tensile strength than AVNP-2 (Figure 6B) loaded bandage samples while the ultimate strain of AVNP-2 loaded samples is higher than the UHNP-1 loaded bandage samples. Moreover, the highest tensile strength of UHNP-1 loaded bandage samples for 1 wt% loading was 0.99 ± 0.06 MPa with an ultimate strain of 2.6% (Figure 6A) when compared with 0.19 ± 0.01 MPa and 6.4% for BC:PMMA (Figure 6A,B) bandage samples, and 0.56 ± 0.05 MPa and 3.7% (Figure 6B) for 1 wt% AVNP-2 bandage samples. BC has a high electron donor ability.[34] Therefore, the CH_2-OH groups of BC can act as an electron donor and the hydrogen of PMMA as an electron acceptor and this interaction encourages a dipole–dipole attraction among the two phases, which can enhance the molecular interaction.[35] However, this interaction has a larger intermolecular gap, which leads to a decrease in the ultimate tensile strength value on the BC:PMMA sample. The ultimate tensile strength of the UHNP-1 and AVNP-2 loaded bandage samples exhibited a steady rise with increased proportions of UHNP-1 and AVNP-2. It is suggested that the colloid phase of these antimicrobial nanoparticles is expected to somewhat fill the intermolecular gaps and hence can help create an increasing trend on the ultimate tensile strength. Atar-Froyman et al.[36] used non-release polycationic antimicrobials by crosslinking of the PMMA polymer and the ultimate tensile of the produced films were in the range of 0.2 and 0.15 MPa, which are lower than this present work's ultimate tensile values for both UHNP-1 and AVNP-2 loaded bandage samples. Additionally, the percentage elongation at break of the gyrated fibers showed a decreasing trend with increasing proportion of UHNP-1 and AVNP-2, from 13 ± 0.20% for BC:PMMA sample to 5.60 ± 0.20 and 3.10 ± 0.10% for UHNP-1 and AVNP-2 loaded samples, respectively. These results indicate that the adding of antimicrobial nanoparticles can improve the interconnection of gyrated fibers, which can be beneficial for the enhancement of ultimate tensile strength while decreasing both ultimate strain and percentage of elongation at break.

Elasticity is one of the most important parameters for bandage like scaffolds for their practical applicability.

Table 2. Mechanical properties of BC:PMMA bandage samples with addition of UHNP-1 and AVNP-2.

Sample name	Ultimate tensile strength [MPa]	Young's modulus [MPa]	Elongation at break [%]
BC:PMMA	0.19 ± 0.01	0.03 ± 0.01	13 ± 0.20
0.05 UHNP-1	0.45 ± 0.03	0.08 ± 0.01	9.50 ± 0.15
0.1 UHNP-1	0.56 ± 0.09	0.14 ± 0.01	8.60 ± 0.07
0.5 UHNP-1	0.76 ± 0.10	0.21 ± 0.06	6.20 ± 0.06
1 UHNP-1	0.99 ± 0.06	0.38 ± 0.05	5.60 ± 0.20
0.05 AVNP-2	0.27 ± 0.04	0.05 ± 0.01	4.60 ± 0.20
0.1 AVNP-2	0.34 ± 0.06	0.07 ± 0.04	4.20 ± 0.35
0.5 AVNP-2	0.42 ± 0.07	0.09 ± 0.03	3.60 ± 0.32
1 AVNP-2	0.56 ± 0.05	0.15 ± 0.04	3.10 ± 0.10

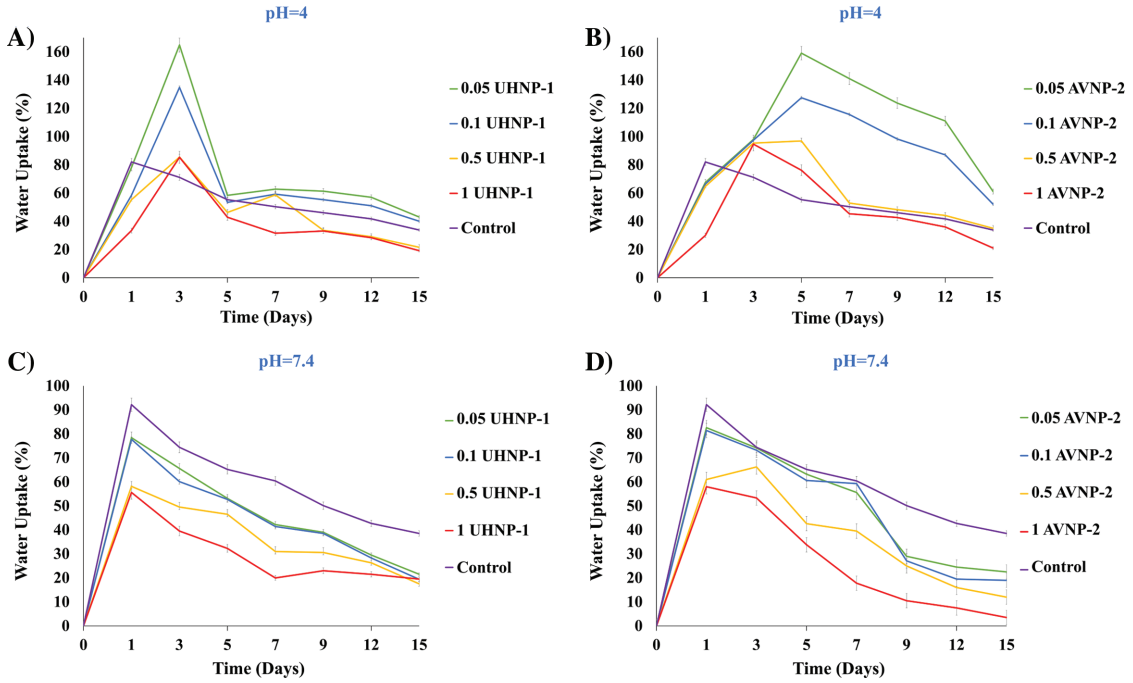

Figure 7. Comparative water uptake properties of all bandage samples including control sample (BC:PMMA) in PBS at A,B) pH 4 and C,D) 7.4.

Therefore, since direct application on the skin is aimed, bandage like scaffolds should have similar mechanical features in order to be compatible with its surroundings.[37] Thus, this synergy can also support the compatibility in the cellular manner due to ensuring similar environmental factors since the skin is constantly in motion caused by the movements of the bearer and therefore, scaffolds designed to host cell adhesion needs to be enduring and corresponding to the motion. This can be ensured by having proper Young's modulus values. In this sense, PMMA has very inappropriate Young's modulus due to its glassy nature, while BC shows higher flexibility. To investigate the influence of UHNP-1 and AVNP-2 on the mechanical properties of bandage samples, Young's modulus was evaluated. The maximum Young's modulus increased with increasing UHNP-1 and AVNP-2 portions in the bandage samples. As can be seen in Table 2, Young's modulus of the bandage like scaffolds produced in this study was in the range of 0.03 ± 0.01 MPa to 0.38 ± 0.05 MPa increasing in parallel with the presence of antimicrobial nanoparticles. Young's modulus of the native human skin is reported to be 0.1–0.85 MPa, as measured by different methods under different circumstances such as age, humidity and temperature.[38] Therefore, the results suggested that UHNP-1 loaded bandage samples are much flexible and promising in terms of elasticity to meet the required elasticity level of the skin compared to AVNP-2 loaded samples.

The capacity to maintain a moisture absorbing environment is a crucial factor for wound dressing materials and according to previous studies BC addition increases the water absorbance and wicking ability.[39,40] In this study, water uptake behavior of the bandage samples within PBS for both 4 and 7.4 pH grades were investigated for all BC:PMMA bandage samples with UHNP-1 (**Figure 7**A,C) and AVNP-2 (Figure 7B,D). The pH environment of chronic wounds is in the range 7.2–8.9, while the wound progresses towards healing; the pH of the underlying tissue moves to neutral and then becomes more acidic.[41,42] For these reasons PBS with both 4 and 7.4 pH grades were used in our tests to understand the water uptake ability of the bandages at both pH values. When the water absorption capacity of the bandages increase, exudates will be absorbed, the wound will remain dry and airborne infection will be prevented. The addition of UHNP-1 and AVNP-2 increased the water uptake ability of bandages at pH 4, while decreasing the water uptake ability at pH 7.4. Decrease in water uptake was observed at higher concentrations of UHNP-1 and AVNP-2 for both 4 and 7.4 pH. This can be caused by the binding of UHNP-1 and AVNP-2 antimicrobial nanoparticles with electron rich 'O' atoms of hydroxyl groups present in BC.

The degradation behavior of UHNP-1 and AVNP-2 loaded BC:PMMA bandage samples were investigated by placing the samples in PBS at pH 4 and 7.4. **Figure 8** shows the weight loss of the samples. The addition of UHNP-1 (Figure 8A,C) and AVNP-2 (Figure 8B,D) decreased the weight loss of bandages at both pH values and suggest that UHNP-1 and AVNP-2 loaded BC:PMMA bandages are highly biodegradable under wound healing conditions. It has been reported that the biodegradation rate of PMMA is relatively slow and that provides durability to the PMMA polymer and make them excellent tissue scaffolds.[43] This feature also has been attributed with the hydrophobic nature of the PMMA.[44] However, increasing the rate and speed of the biodegradation can be beneficial depending on the application type and target of the tissue scaffolds. This statement is especially important for the wound dressing bandages due to the fact that bandages are not designed for longer periods of usage. In this work, bandages were subjected to the two different environments with varying pH grades (7.4 and 4)

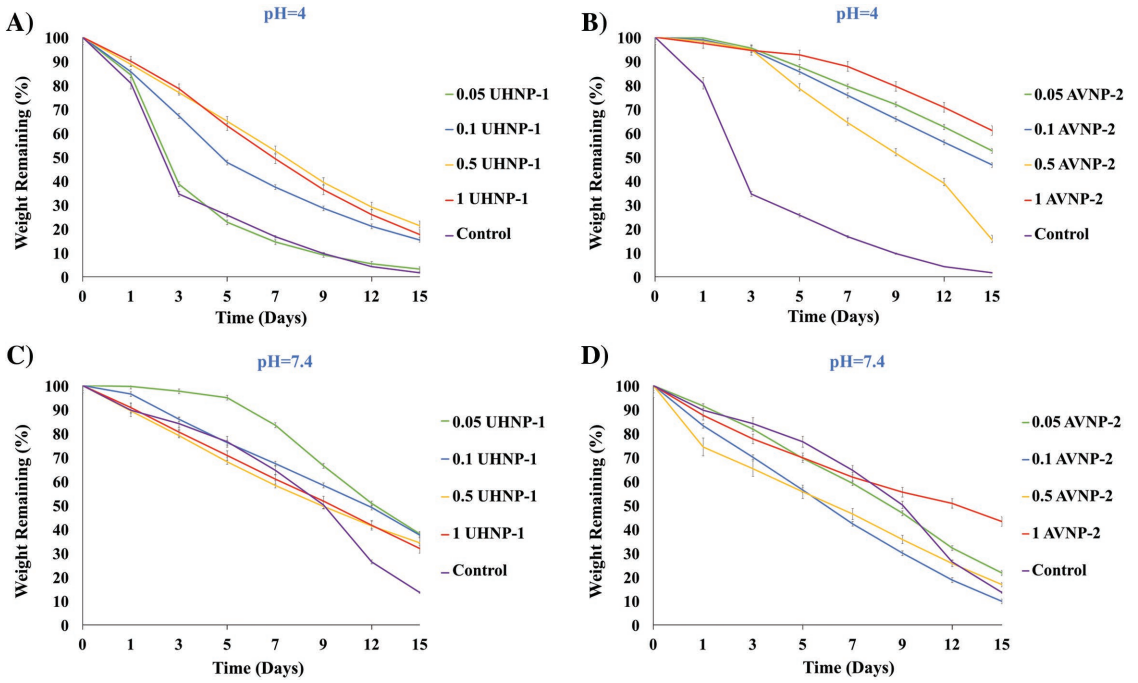

Figure 8. Comparative weight loss properties of all bandage samples including control sample (BC:PMMA) at A,B) pH 4 and C,D) 7.4.

and results indicated that the biodegradation rate was increased when the environmental features shifted to a more acidic condition. Nevertheless, the only reason for fluctuations in biodegradation of the BC:PMMA bandages cannot be explained solely with the pH factor. Dipole–dipole attraction between the BC and PMMA molecules are also an important factor and this can result in higher degradation rates, which will eventually lead to increased weight loss.[45] This can justify the extreme weight loss of the BC:PMMA bandages compared to other studies and against the well accepted reputation of the low biodegradability of PMMA scaffolds. Nevertheless, due to mechanics of the fiber formation via pressurized gyration processes, bandages can contain a more anisotropic fiber which is dissimilar to other fiber production methods.[27] During the biodegradation test, it has been observed that the bandage samples tended to slightly break apart, which increases the surface ratio of the material, increasing biodegradation eventually.[46] It is believed that this behavior can be related to the production method, unique fiber formation and shape of the bandages. Even though this can be considered as a challenging aspect in other applications, where longer periods of structural integrity is required, biodegradation behavior of the bandages has been evaluated for 15 days and results can be considered significantly promising since the good biocompatibility has been successfully combined with rapid biodegradation, which will enable the native cells of the body proliferate while they are being supported by constantly degrading scaffolds and eventually take over the control of the wound area by the degradation of the bandage scaffolds.

Figure 9 shows the DSC curves of virgin BC, virgin PMMA, and the bandage samples prepared from their blends incorporating the two typical antimicrobial nanoparticles. While virgin BC exhibited no T_g, which is due to the its extremely hard and un-relaxable chain structure, highly amorphous virgin PMMA, which is the major constituent in the matrix of the bandage samples exhibited a characteristic T_g at 106 °C. It is worth noting that, all the bandage samples and the physical blend of BC and PMMA exhibited only one T_g belonging to their PMMA part due to compatibility of blend components. Integration of these two polymeric phases shifted the T_g to 121 °C, which is considerably higher than that of the virgin PMMA. This bears proof of molecular interactions between BC and PMMA, eventually pushing the T_g to higher levels. This effect is also correlated with the formation of hydrogen bonding in the polymeric phases.[47,48] Increase in T_g of the blend was due to the hydrogen bonding formed between −C=O groups of PMMA and CH_2−OH groups of BC, which hindered the relaxation and

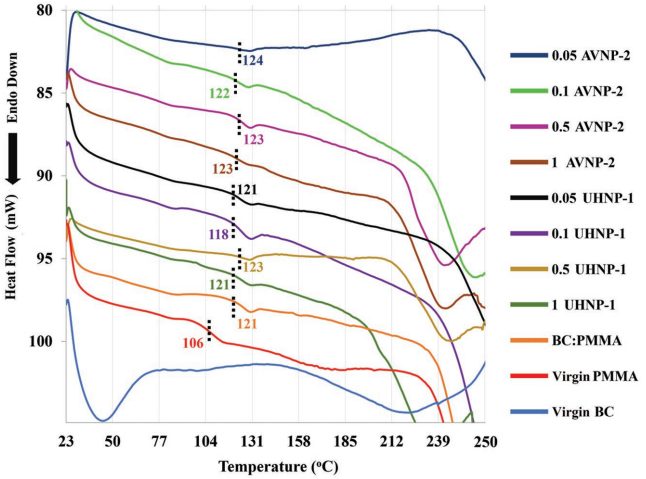

Figure 9. DSC thermograms of the bandage samples, endotherms are indicated as troughs.

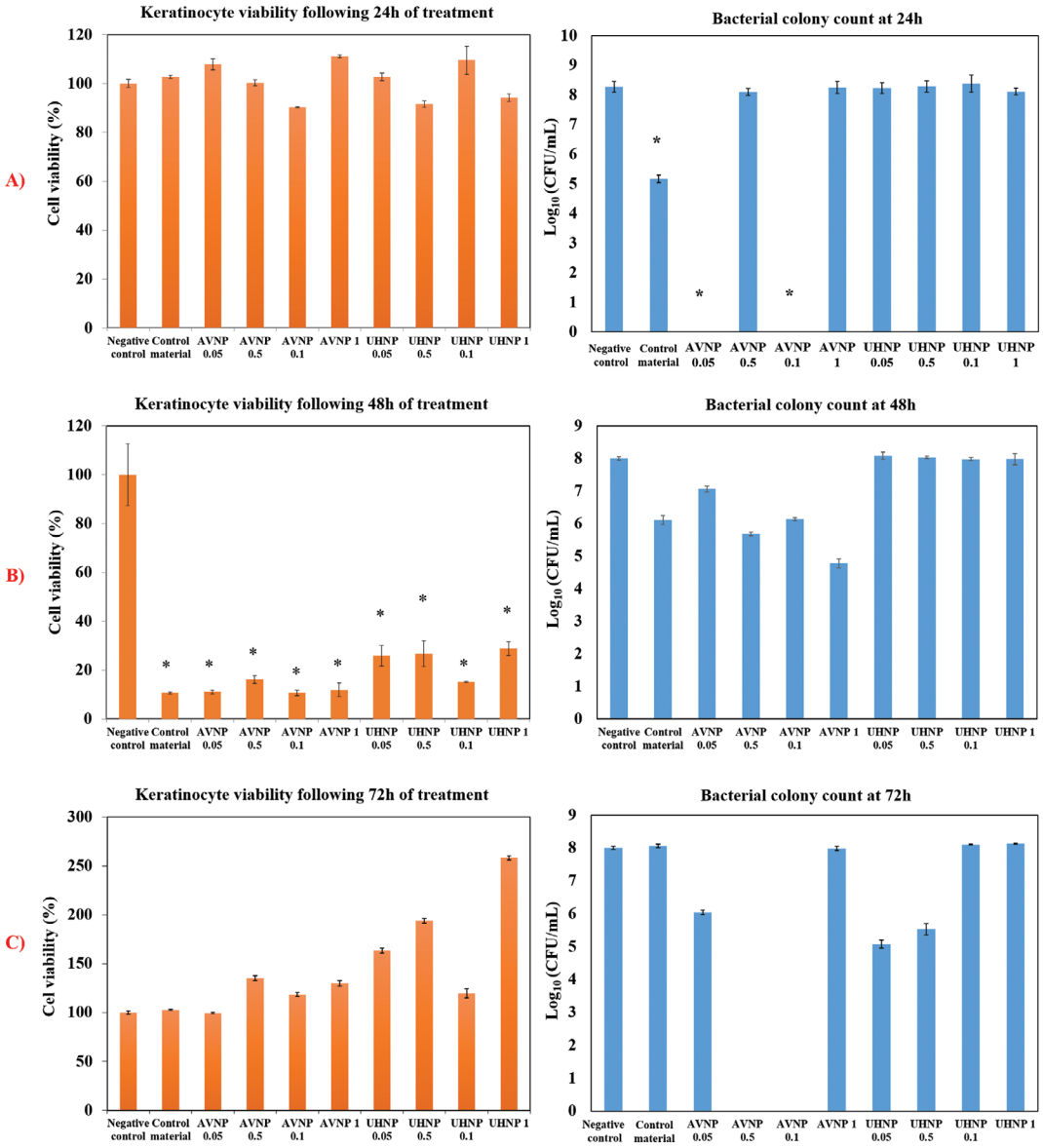

Figure 10. Cell viability and bacterial colony counts following co-culture with the control material (BC:PMMA), UHNP-1 and AVNP-2 materials. MTT analysis and colony counts were performed following A) 24 h, B) 48 h, and C) 72 h of co-culture. Data are the means ± S.D.; $n = 3$, ANOVA. *$p < 0.05$ versus negative control.

Figure 11. Fluorescence microscopy images of A) control material (BC:PMMA), B) UHNP-1, and C) AVNP-2 attached keratinocytes cells with DAPI stained nuclei.

rotational motion of the PMMA main chain. However, antimicrobial nanoparticles used in this work did not influence the thermal properties as these elements (Cu, Ag, W) cannot form hydrogen bonds with polymeric materials. Therefore, regardless of the type and concentration of the antimicrobial samples used, T_g remained stable in a very small range (121–124 °C). Normal body temperature is ≈37 °C with skin slightly cooler than the body temperature due to its location and limitless contact with air and body heat loss. On the other hand, temperatures above 40 °C are considered to be life-threatening. Thus, DSC results indicate bandage samples produced in this study will not pose temperature related problems and are safe to use as wound dressings.

In the case of wounds, human skin is the first line of defense against pathogenic bacteria. The exterior level of the skin, epidermis, is predominantly composed of keratinocyte cells and functions as a physical barrier to threats.[49] Therefore, keratinocytes were selected to examine the biocompatibility of the bandage samples. The biocompatibility of the different ratio of UHNP-1 and AVNP-2 nanoparticles loaded BC:PMMA composite fiber bandages were evaluated by co-culturing with Keratinocytes and *S. aureus* ATCC29213 bacterial cells for 24, 48, and 72 h. Cell proliferations and colony count changes are shown in **Figure 10**. *S. aureus* ATCC29213 in co-culture with keratinocytes serve as model system for infected wounds. After co-culturing for 24 h (Figure 10A), the viability of keratinocytes did not show a considerable change with any of the nanoparticles. It is also clearly seen that the presence of AVNP-2 nanoparticles causes a significant decrease of *S. aureus* ATCC29213 at 24 h. At 48 h, the number of viable keratinocytes decreased with all nanoparticles including control material in Figure 10B. *S. aureus* ATCC29213 bacterial colony counts at 48 h slightly decrease with increasing concentrations of AVNP-2 nanoparticles compared to the control material, however there were no significant differences for the concentrations of UHNP-1 nanoparticles tested (Figure 10B). Cells continued growth in well spread ways at 72 h, those have comparable higher concentrations of UHNP-1 nanoparticles caused an increase in cellular activity compared to AVNP-2 nanoparticles (Figure 10C). Fluorescence microscopy images of control material (BC:PMMA), UHNP-1, and AVNP-2 attached keratinocytes cells with DAPI stained nuclei are represented in **Figure 11**. In addition, *S. aureus* ATCC29213 bacterial colony counts highlighted that 1 wt% UHNP-1 and 1 wt% AVNP-2 loaded BC:PMMA composite fiber bandages were similar to the control material. The antimicrobial nanoparticle mechanism of action is not completely clear. However, their potential application in biomedical researches has led to a high level of research activity to determine the safety and efficacy of these nanoparticles for antimicrobials in clinical applications. Commonly agreed mechanism of antimicrobial nanoparticles hypothesize of action within which the nanoparticles are positively charged and can be very useful in disruption and destructive towards the bacterial cell-walls. This disruption to cell walls can lead directly to a damage against bacterial surface envelop structures. The surface damage may cause substantial H^+ leakage that results in eventual disruption of membrane potential at sub-micromolar concentrations. And these would result ultimately in the death of the microbe or the bacterial cell death.[16,50,51]

In the co-culture system bacterial colonies were observed on the control material (BC:PMMA) as shown in **Figure 12**A. SEM images (Figure 12B,C) showed that there were almost no bacterial cells due to the presence of the 1 wt% UHNP-1 and 1 wt% AVNP-2, indicating that both nanoparticles delivered antibacterial activity. In addition, Figure 12C clearly shows typical keratinocyte cells growing on 1 wt% AVNP-2 loaded BC:PMMA fiber bandages.

AVNP-2 loaded BC:PMMA bandages seem to be more active in terms of antibacterial effects when compared to UHNP-1

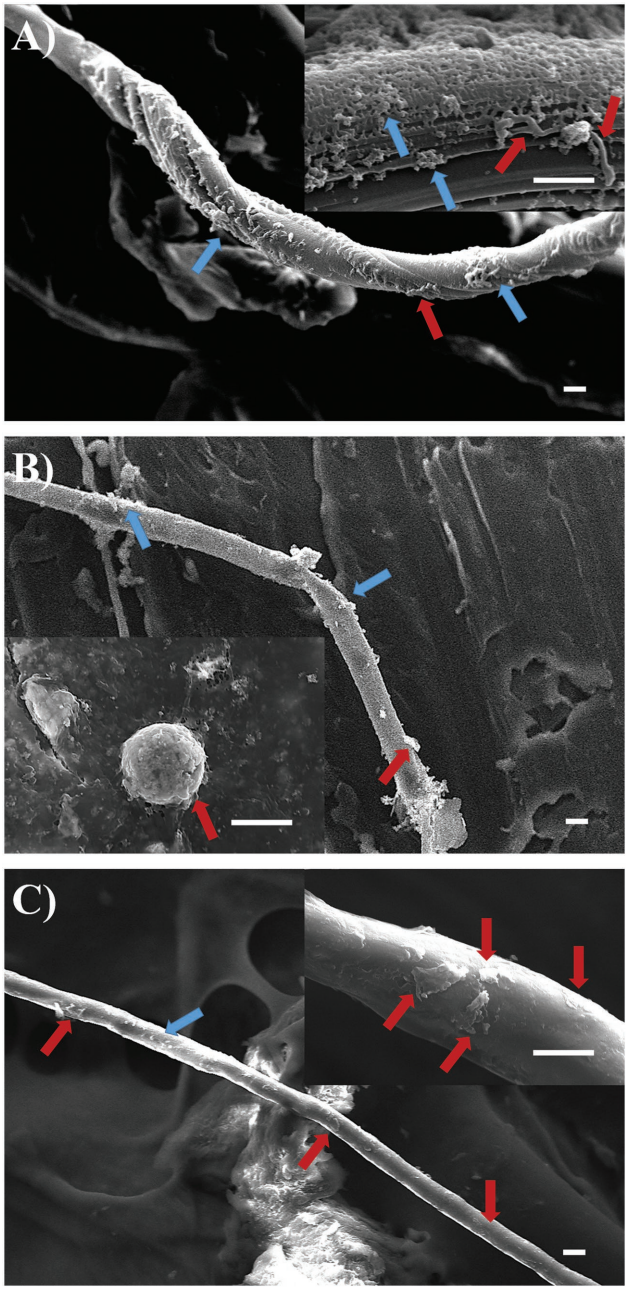

Figure 12. SEM images of bandage samples after cell viability (indicated with red arrows) and bacterial colony counts (indicated with blue arrows) following co-culture. A) Control material (BC:PMMA), B) 1 UHNP-1, and C) 1 AVNP-2. (Scale bars indicate 10 µm).

counterparts and expressed better or similar results obtained with the control material. AVNP-2 loaded BC:PMMA bandages can promote physiological conditions for wound healing and establish a barrier against pathogen microorganisms such as *S. aureus*.

4. Conclusions

In summary, novel BC:PMMA bandages were prepared by pressurized gyration. Different amounts of UHNP-1 and AVNP-2 were added into the BC:PMMA as antimicrobial nanoparticles and had a significant effect on the properties of the bandage samples. Resulting bandages were manufactured with high product yield. Increased density in solutions with additional antimicrobial nanoparticles resulted in increased fiber diameters. The typical molecular bonding in the bandages was confirmed by FTIR, with the peaks that have higher intensity and narrowing points which were caused by the addition of antimicrobial nanoparticles. Molecular interaction was also proven by the T_g values measured in the DSC tests, where bandage samples were found suitable to be used as wound dressings without compromising their integrity against thermal conditions of the natural environment. Tensile tests showed UHNP-1 loaded bandage samples were more flexible and promising in terms of elasticity compared to AVNP-2 loaded samples. Decrease in water uptake and weight loss of bandages were observed with increased concentrations of UHNP-1 and AVNP-2 (from 0.05 to 1 wt%). In the co-culture system with Keratinocytes and *S. aureus* ATCC29213 bacterial colonies, AVNP-2 loaded bandage samples showed significant higher cell viability and bacteria inhibition during co-culture times of 24–72 h. AVNP-2 loaded BC:PMMA bandages can promote physiological conditions for wound healing and establish a barrier against pathogen microorganisms such as *S. aureus*. The results of in vitro co-culture test proved that the bandages containing UHNP-1 and AVNP-2 antimicrobial nanoparticles have a promising future as epidermal wound dressing materials.

Acknowledgements

The authors wish to thank UCL for part supporting the visits of Esra Altun and Mehmet Onur Aydogdu. The authors also wish to thank the Engineering and Physical Sciences Research Council UK for supporting gyration spinning work at UCL (Grants EP/L 023059/1, EP/N 034228/1). Data supporting this paper are in the paper and in our short communication (DOI: 10.1002/mame.201800577) (reference 12).

Conflict of Interest

The authors declare no conflict of interest.

Keywords

antimicrobial metallics, bacterial cellulose, bandage properties, cellular and bacteria co-cultures, polymers

Received: September 3, 2018
Revised: October 26, 2018
Published online: November 28, 2018

[1] G. Majno, *The Healing Hand: Man and Wound in the Ancient World*, Harvard University Press, Cambridge, UK **1975**.
[2] C. Daunton, S. Kothari, L. Smith, D. Steele, *Wound Pract. Res.* **2012**, *20*, 174.
[3] V. Jones, J. E. Grey, K. G. Harding, *BMJ* **2006**, *332*, 777.
[4] L. Zhang, P. Xu, X. Wang, M. Zhang, Y. Yan, Y. Chen, L. Zhang, L. Zhang, *Int. J. Biochem. Cell Biol.* **2017**, *87*, 69.
[5] T. Gunasekaran, T. Nigusse, M. D. Dhanaraju, *J. Am. Coll. Clin. Wound Spec.* **2011**, *3*, 82.
[6] M. Woodward, *Prim. Inten.* **2005**, *13*, 153.
[7] G. Borkow, N. Okon-Levy, J. Gabbay, *Wounds* **2010**, *22*, 301.
[8] D. Klemm, D. Schumann, U. Udhardt, S. Marsch, *Prog. Polym. Sci.* **2001**, *26*, 1561.
[9] W. C. Lin, C. C. Lien, H. J. Yeh, C. M. Yu, S. H. Hsu, *Carbohydr. Polym.* **2013**, *94*, 603.
[10] M. H. Kwak, J. E. Kim, J. Go, E. K. Koh, S. H. Song, H. J. Son, H. S. Kim, Y. H. Yun, Y. J. Jung, D. Y. Hwang, *Carbohydr. Polym.* **2015**, *122*, 387.
[11] I. Reiniati, A. N. Hrymak, A. Margaritis, *Crit. Rev. Biotechnol.* **2017**, *37*, 510.
[12] E. Altun, M. O. Aydogdu, F. Koc, M. Crabbe-Mann, F. Brako, R. Kaur-Matharu, G. Ozen, S. E. Kuruca, U. Edirisinghe, O. Gunduz, M. Edirisinghe, *Macromol. Mater. Eng.* **2018**, *303*, 1700607.
[13] H. T. Hsieh, H. M. Chang, W. J. Lin, Y. T. Hsu, F. D. Mai, *Sci. Rep.* **2017**, *7*, 9531.
[14] M. R. Ayatollahi, M. R. M. Aliha, M. M. Hassani, *Mater. Sci. Eng., A* **2006**, *417*, 348.
[15] C. Bankier, Y. Cheong, S. Mahalingam, M. Edirisinghe, G. Ren, E. Cloutman-Green, L. Ciric, *PLoS One* **2018**, *13*, e0192093.
[16] G. Ren, D. Hu, E. W. C. Cheng, M. A. Vargas-Reus, P. Reip, R. P. Allaker, *Int. J. Antimicrob. Agents* **2009**, *33*, 587.
[17] Y. K. Cheong, X. Yang, R. M. Wilson, G. Ren, *NanoBio&Med,* Nov **2017**, 105.
[18] X. Liu, P. Y. Lee, C. M. Ho, V. C. Lui, Y. Chen, C. M. Che, P. K. Tam, K. K. Wong, *Chem. Med. Chem.* **2010**, *5*, 468.
[19] S. Zhang, X. Liu, H. Wang, J. Peng, K. K. Wong, *J. Pediatr. Surg.* **2014**, *49*, 606.
[20] K. K. Wong, S. O. Cheung, L. Huang, J. Niu, C. Tao, C. M. Ho, C. M. Che, P. K. Tam, *Chem. Med. Chem.* **2009**, *4*, 1129.
[21] Y. K. Cheong, J. Calvo-Castro, L. Ciric, M. Edirisinghe, E. Cloutman-Green, U. E. Illangakoon, Q. Kang, S. Mahalingam, R. K. Matharu, R. M. Wilson, G. Ren, *Nanomaterials* **2017**, *7*, 152.
[22] G. Ren, J. S. Oxford, P. W. Reip, R. Lambkin-Williams, A. Mann (Queen Mary University of London), *PCT/GB2007/000542*, **2007**.
[23] S. Mahalingam, M. Edirisinghe, *Macromol. Rapid Commun.* **2013**, *34*, 1134.
[24] X. Hong, S. Mahalingam, M. Edirisinghe, *Macromol. Mater. Eng.* **2017**, *302*, 1600564.
[25] S. Zhang, B. T. Karaca, S. K. VanOosten, E. Yuca, S. Mahalingam, M. Edirisinghe, C. Tamerler, *Macromol. Rapid Commun.* **2015**, *36*, 1322.
[26] U. E. Illangakoon, S. Mahalingam, K. Wang, Y. K. Cheong, E. Canales, G. Ren, E. Cloutman-Green, M. Edirisinghe, L. Ciric, *Mater. Sci. Eng., C* **2017**, *74*, 315.
[27] P. L. Heseltine, J. Ahmed, M. Edirisinghe, *Macromol. Mater. Eng.* **2018**, *303*, 1800218.
[28] C. L. Casper, J. S. Stephens, N. G. Tassi, D. B. Chase, J. F. Rabolt, *Macromolecules* **2004**, *37*, 573.
[29] S. Mahalingam, B. T. Raimi-Abraham, D. Q. M. Craig, M. Edirisinghe, *Chem. Eng. J.* **2015**, *280*, 344.
[30] S. Ahmad, S. Ahmad, S. A. Agnihotry, *Bull. Mater. Sci.* **2007**, *30*, 31.
[31] Z. Yang, S. Chen, W. Hu, N. Yin, W. Zhang, C. Xiang, H. Wang, *Carbohydr. Polym.* **2012**, *88*, 173.
[32] Y. Qiu, L. Qiu, J. Cui, Q. Wei, *Mater. Sci. Eng., C* **2016**, *59*, 303.

[33] T. A. Khan, K. K. Peh, H. S. Ch'ng, *J. Pharm. Pharmaceutical Sci.* **2000**, *3*, 303.
[34] M. Pommet, J. Juntaro, J. Y. Y. Heng, A. Mantalaris, A. F. Lee, K. Wilson, G. Kalinka, M. S. P. Shaffer, A. Bismarck, *Biomacromolecules* **2008**, *9*, 1643.
[35] H. U. Zaman, J. M. M. Islam, M. A. Khan, R. A. Khan, *J. Mech. Behav. Biomed. Mater.* **2011**, *4*, 1369.
[36] L. Atar-Froyman, A. Sharon, E. I. Weiss, Y. Houri-Haddad, D. Kesler-Shvero, A. J. Domb, R. Pilo, N. Beyth, *Biomaterials* **2015**, *46*, 141.
[37] A. A. Chaudhari, K. Vig, D. R. Baganizi, R. Sahu, S. Dixit, V. Dennis, S. R. Singh, S. R. Pillai, *Int. J. Mol. Sci.* **2016**, *17*, 1974.
[38] L. Liu, D. Tasis, M. Prato, H. D. Wagner, *Adv. Mater.* **2007**, *19*, 1228.
[39] K. Gelin, A. Bodin, P. Gatenholm, A. Mihranyan, K. Edwards, M. Strømme, *Polymer* **2007**, *48*, 7623.
[40] A. Meftahi, R. Khajavi, A. Rashidi, M. Sattari, M. E. Yazdanshenas, M. Torabi, *Cellulose* **2010**, *17*, 199.
[41] K. Tsukada, K. Tokunaga, T. Iwama, Y. Mishima, *Wounds* **1992**, *4*, 16.
[42] T. Kaufman, E. H. Eichenlaub, M. F. Angel, M. Levin, J. W. Futrell, *Burns* **1985**, *12*, 84.
[43] Y. Liu, Y. Ji, K. Ghosh, R. A. Clark, L. Huang, M. H. Rafailovich, *J. Biomed. Mater. Res., Part A* **2009**, *90A*, 1092.
[44] P. K. Sahoo, R. Samal, *Polym. Degrad. Stab.* **2007**, *92*, 1700.
[45] S. Maiti, S. Sain, D. Ray, D. Mitra, *Polym. Degrad. Stab.* **2013**, *98*, 635.
[46] S. Chinagli, M. Tosin, F. Degli-Innocenti, *Polym. Degrad. Stab.* **2018**, *147*, 237.
[47] M. S. Bostan, E. S. Mutlu, H. Kazak, S. S. Keskin, E. T. Oner, M. S. Eroglu, *Carbohydr. Polym.* **2014**, *102*, 993.
[48] T. Caykara, S. Demirci, M. S. Eroglu, O. Guven, *Polymer* **2005**, *46*, 10750.
[49] T. S. Kupper, R. C. Fuhlbrigge, *Nat. Rev. Immunol.* **2004**, *4*, 211.
[50] P. Dibrov, J. Dzioba, K. K. Gosink, C. C. Häse, *Antimicrob. Agents Chemother.* **2002**, *46*, 2668.
[51] J. B. Chappell, G. D. Greville, *Nature* **1954**, *174*, 930.